Journal of Physics D:
Applied Physics

PAPER • **OPEN ACCESS**

Influence of stretching on the properties of laser-induced graphene on polyurethane strain sensors

To cite this article: Cornelia Hoppe *et al* 2025 *J. Phys. D: Appl. Phys.* **58** 445304

OPEN ACCESS
IOP Publishing
Journal of Physics D: Applied Physics
J. Phys. D: Appl. Phys. **58** (2025) 445304 (14pp)
https://doi.org/10.1088/1361-6463/ae1599

Influence of stretching on the properties of laser-induced graphene on polyurethane strain sensors

Cornelia Hoppe[1], **Yu Kyoung Ryu**[1,2,*] **and Javier Martinez**[1,3,*]

[1] Instituto de Sistemas Optoelectrónicos y Microtecnología, Universidad Politécnica de Madrid, Av. Complutense 30, 28040 Madrid, Spain
[2] Departamento de Física Aplicada e Ingeniería de Materiales, E. T. S. I. Industriales, Universidad Politécnica de Madrid, C/José Gutiérrez Abascal 2, 28006 Madrid, Spain
[3] Departamento de Ciencia de Materiales-CIME, E. T. S. I. Caminos, Canales y Puertos, Universidad Politécnica de Madrid, C/Profesor Aranguren s/n, 28040 Madrid, Spain

E-mail: y.ryu@upm.es and javier.martinez@upm.es

Received 31 July 2025, revised 22 September 2025
Accepted for publication 21 October 2025
Published 30 October 2025

Abstract

In today's digital age, the interest in wearable electronics has been growing distinctively. However, the fabrication of lightweight, stretchable and reasonably priced conductors is still challenging. Due to its high electrical conductivity, and three-dimensional porous structure, laser-induced graphene (LIG) is predestined as one of the active materials of choice in flexible sensors. With the laser-induced transformation of carbonic precursors, a low-cost, time-efficient, facile and scalable production technique of graphene like materials has emerged. Herein, we used this method to generate LIG on the surface of polyimide (PI) using a CO_2 laser with a wavelength of 10.6 μm and subsequently transferring the pattern to Fixomull®, a commercial medical grade polyurethane. Afterwards, a detailed characterization of the elastomeric conductive polymer composite LIG/Fixomull under different deformation levels was performed. Scanning electron microscopy (SEM), Raman spectroscopy and van der Pauw sheet resistance measurements gave a better understanding of the performance of the LIG-based strain sensor as a function of the stretching degree in correlation to the changes that the porous structure of the material was undergoing. Our flexible LIG/Fixomull sensor demonstrates high stretchability of min. 80%, a linear range up to 30% strain and reliable data acquisition up to 60% strain, as well as a stable signal output for 20 subsequent stretch-release cycles to 30% strain.

Supplementary material for this article is available online

Keywords: laser-induced graphene, polyurethane, stretchable conductors, strain sensors

* Authors to whom any correspondence should be addressed.

1. Introduction

With the advancement of the internet of things (IoTs), smart devices are also being implemented into the medical field [1, 2], giving rise to the internet of medical things (IoMTs) [3]. To be precise, health care is, amongst the common relevant economic sectors, the one with the highest practical implementation rate of IoT applications [4]. This means that smart medical services have currently even greater practical relevance than IoT systems in the automated manufacturing sector [4].

Collection and real-time transmission of health data would allow for remote health monitoring & diagnosis as well as infectious disease tracking, improving emergency care and medical services [3, 5, 6]. This development requires availability of high-performing wearable electronics on a large scale [7].

Demands on sensor devices for health data collection are broad, including high stretchability [2, 8–10], sensitivity [2, 8–10], stability [2, 9, 10], breathability [10] and skin compatibility [9, 10], a low weight [2], large sensing range [8], fast response time [8] and a facile fabrication [9, 10].

With their report on a laser-based fabrication process [11], Lin *et al* have made an essential contribution in the development towards readily available wearable strain sensors [1], proposing a fast, controllable, cost-effective and scalable method to produce graphene [5, 11]. The resulting LIG with its outstanding electrical properties [12], high porosity, hence huge specific surface area of $\sim$2600 m^2 g^{-1} [13], biocompatibility [14], reversible strain up to 25% [15] and possibility to be transferred to a wide range of elastomeric substrates [10, 16], is predestined to be applied in sensor devices.

Applicability of conventional metal- and semiconductor-based sensors in IoMT devices is limited owing to their inherently low dynamic sensing range ($\leqslant$5% strain), complex fabrication and rigidity [1, 2, 5]. Meanwhile, wearable electronics composed of laser-induced graphene (LIG) embedded in an elastomer substrate have proved high potential for sensing applications [2, 7]—not only for health monitoring but also for environmental monitoring and human machine interface applications [7, 8]. With a Young's modulus in the range of 10 kPa–10 MPa [17], a typical elastomer brings along the desired mechanical properties, most importantly a high flexibility and high toughness [10], while the graphene introduces excellent electrical properties owing to the delocalized π-system that elicits an exceptionally high carrier mobility $>$200.000 cm^2 $(V * s)^{-1}$, i.e. very high electrical conductivity [12, 18]. Under this configuration, the theoretically optimal wearable electronic device is created [10, 17].

LIG-based strain sensors can be attached to any part of the human body (elbow, biceps, wrist, finger, throat, mouth, eyebrow) for monitoring a wide range of human body motions [1, 8]: from vocal vibration and physiological pulse, categorized as subtle movement and causing ultra-small strain $<$1% to joint movements in the middle-high strain region with $\sim$60% strain caused by finger movement and $\sim$100% strain caused by knee movement [1]. Sensors for this purpose not only need the ability to detect an ultrawide strain range from less than 0.1% to more than 100% but also a high time resolution (of the signal), stability against a range of operational conditions [7], high sensitivity and accuracy [1].

The underlying physical principle of data collection is the piezoresistive effect. Strain information, induced by relaxation and contraction of human muscles upon movement causes the conductive graphene pathway to be partially interrupted. This reflects itself in a change in electrical resistance that in turn can be measured [1, 8].

This study aims to provide a complete material characterization of LIG embedded in the elastomeric substrate polyurethane and strained to defined levels. As complement to extensive electromechanical characterizations of LIG-based sensor devices, addressed in different studies [1, 8, 10, 17, 19], a deeper understanding of the structural changes that the material system itself is undergoing, independent of the wiring or other components of the final sensor device, should be gained.

Besides, the chosen alternative substrate material Fixomull is assessed in comparison to the more investigated substrate polydimethylsiloxane (PDMS). While there are several studies on LIG/PDMS strain sensors proving their high sensitivity, good repeatability, short response, and recovery time [8, 20, 21], investigations of different substrate materials with potential complementary/alternative benefits are more limited yet. We study polyurethane which has a very high stretchability (elongation break $>$400% [10]), low thickness and excellent skin compatibility [22]. Moreover, first long-term tests by Dallinger *et al* and Kammarchedu *et al* have demonstrated a reliable performance of LIG/Fixomull strain sensors over 200 cycles to 30% strain [10] and even over 10 000 cycles to 5% strain [16], respectively. These results promise a high sensor stability that is of great value with regard to application in actual sensing devices for everyday use.

The substrate used in this work is commercially available medical grade polyurethane (MPU), Fixomull, which is a wound care product and thus designed for long-term & conformal adhesion on skin (up to seven days according to the manufacturer) even when exposed to water, which implies breathability and hydrophobicity [23]. The exceptionally high stretchability, the low thickness, skin compatibility, breathability and promising stability make Fixomull an excellent substrate choice for application in LIG-based strain sensors to be worn on skin. On the other hand, the biosafety of LIG has been demonstrated in studies by d'Amora *et al* and Huang *et al* based on extensive *in vivo* experiments with zebrafish and rats [24, 25]. Therefore, the biocompatibility of the final LIG/Fixomull composite is substantiated.

Scanning electron microscopy (SEM) images illustrated a distinctly intensified interruption of the conductive LIG paths for strains $\geqslant$40% and Raman spectra exhibited a fundamental change in chemical structure for this strain level, suggesting an incipient amorphization of the LIG. Van der Pauw measurements showed an order of magnitude increase in the sheet resistance value after the transfer of the LIG from Kapton to Fixomull, but similar values in the range of after transfer to 15% and only a factor 2 increase of the value in the range of

20%–80%. Electromechanical characterization yielded a linear sensing range of the fabricated sensors of up to 30% and a close-to-linear relationship between sensor output signal and applied strain for up to 60%. The stability of the sensor was tested by 20 subsequent stretch-release cycles to 30% strain.

2. Methodology

2.1. LIG synthesis and transfer to polyurethane

Figure 1(a) schematically illustrates the photothermal process applied to generate LIG: patterns were scribed under ambient conditions onto ethanol-cleaned PI films (Kapton® HN film, DuPont™, thickness of 50 μm–in the following referred shortly as Kapton) with a commercial, hobby-grade IR CO_2 laser with a wavelength of 10.6 μm, a maximum power of 40 W and a maximum scanning speed of 600 mm s^{-1}. The applied laser parameters were optimized based on previous investigations by our research group [26, 27], by Kammarchedu *et al* [16] and Dallinger *et al* [10] and found to yield best performing fibrous LIG for a laser power of 3.2 W and a scanning speed of 110 mm s^{-1} in this work. By varying the laser fluence, set to convert the upper atomic layers of the carbonic precursor [28], the morphology and with it, the properties of LIG can be tuned in a wide range according to the desired application [29]. Here, a fibrous morphology was aspired as LIG fibers have been proven to tolerate large strains and promote subsequent transfer to an elastomeric substrate [10, 16]. The beam movement in *X*- and *Y*-direction was controlled by the software K40 Whisperer according to the pre-specified pattern that was designed with the vector graphics software Inkscape. The Z-coordinate was kept constant throughout the irradiation such that the laser operated at focal plane with the devicès focused beam size of 100 μm as determined by Velasco *et al* [26]. A scanline step of 76.2 μm was employed in raster mode, for which the two-dimensional LIG pattern was created by irradiating the Kapton line by line in *X*-direction.

As depicted by the photo series in figure 1(b), pieces of Kapton film were attached onto an aluminum plate using adhesive Kapton tape and transformed into LIG with the parameters specified above. Subsequently, a piece of Fixomull was attached to the exposed LIG with its polyacrylate adhesive side. Fixomull® transparent (BSN medical GmbH, Germany) is a commercially available MPU that has polyacrylate glue applied to the actual polyurethane layer (overall thickness of ∼54 μm), with the polyacrylate glue being protected by a glassine paper and the polyurethane by a plastic liner.

In order to promote good adhesion of the Fixomull to LIG and thereby maximize the amount of transferred material, moderate pressure was applied with a cotton tip. Next, the Fixomull was peeled off in one continuous movement, resulting in a good amount of LIG being embedded in Fixomull and some residual LIG remaining on Kapton, which is shown in the right picture of figure 1(b).

The whole fabrication process was conducted under ambient conditions.

2.1.1. Preparation of samples for the structural characterization techniques. Samples for the stretch series were prepared by simply straining the LIG/Fixomull samples to the following defined levels: 5%, 10%, 15%, 20%, 25%, 30%, 40%, 60%, 80% with one sample remaining unstretched (0%). The strain levels were determined such that a high number was assumed to lie within the linear regime of a LIG/Fixomull sensor as identified by Keller *et al* and Dallinger *et al* [10, 17]. The LIG pattern chosen for SEM and Raman spectroscopy was the same 20 × 10 mm^2 serpentine pattern used for the sensors depicted in figures 1(b) and a Greek cross structure for van der Pauw sheet resistance measurements. The straining was performed with a manual 500 N digital push pull force gauge (HP series, Mxmoonfree). Each sample was stretched to the specified strain level three times in a row with a dwell time of 60 s in each state (released/ strained).

2.1.2. Preparation of sensors for the electromechanical tests. A sensor with basic electrical wiring was assembled in order to perform some fundamental electromechanical measurements to link the electric and the mechanical response of the sensors during stretching by applying simultaneously strain with the force gauge and tracking the changes in the resistance through linear sweep voltammetry (LSV) and chronoamperometry tests. For this purpose, the serpentine pattern chosen to further enhance flexibility and deformability of LIG [17, 30] was transferred to Fixomull as described in figure 1(b). Subsequently, copper wires were attached to the designated LIG contact pads using conductive silver paste and small pieces of adhesive copper tape for fixing. Finally, a second layer of Fixomull was stuck on top, including the wiring, resulting in the LIG sensor sandwiched between the elastomer substrates. The fabricated devices can be seen in figures 7(b) and (c) and a close-up picture is provided in figure S1 (supplementary data file).

Due to the anisotropy of LIG patterns that originates from the line-by-line irradiation in combination with the Gaussian-shaped laser beam profile [26], the orientation of the strain application direction relative to the lasing direction needs to be considered carefully. Based on the investigations by Yen *et al*, all samples were fabricated with a parallel structure. That is to say, the strain was applied parallel to the lasing direction as illustrated in figure 1(c), right. As proven by Yen *et al*, parallel LIG strain sensors show a better performance compared to those with a vertical structure in terms of sensor sensitivity, as shown in figure 1(c) [21]. On one hand, the electrical connectivity between neighboring spots within one line is superior to the one between successively written lines resulting in a lower initial resistance in the case of parallel LIG structures [16, 31]. On the other hand, cracks—which doubtlessly form upon increasing strain—will form perpendicular to the straining direction [21], i.e. perpendicular to laser lines for parallel LIG structures (shown in figure 1(c), right) and parallel to laser lines for perpendicular LIG structures (shown in figure 1(c), left). Consequently, the number of conductive paths changes more distinctly upon application of strain in case of parallel

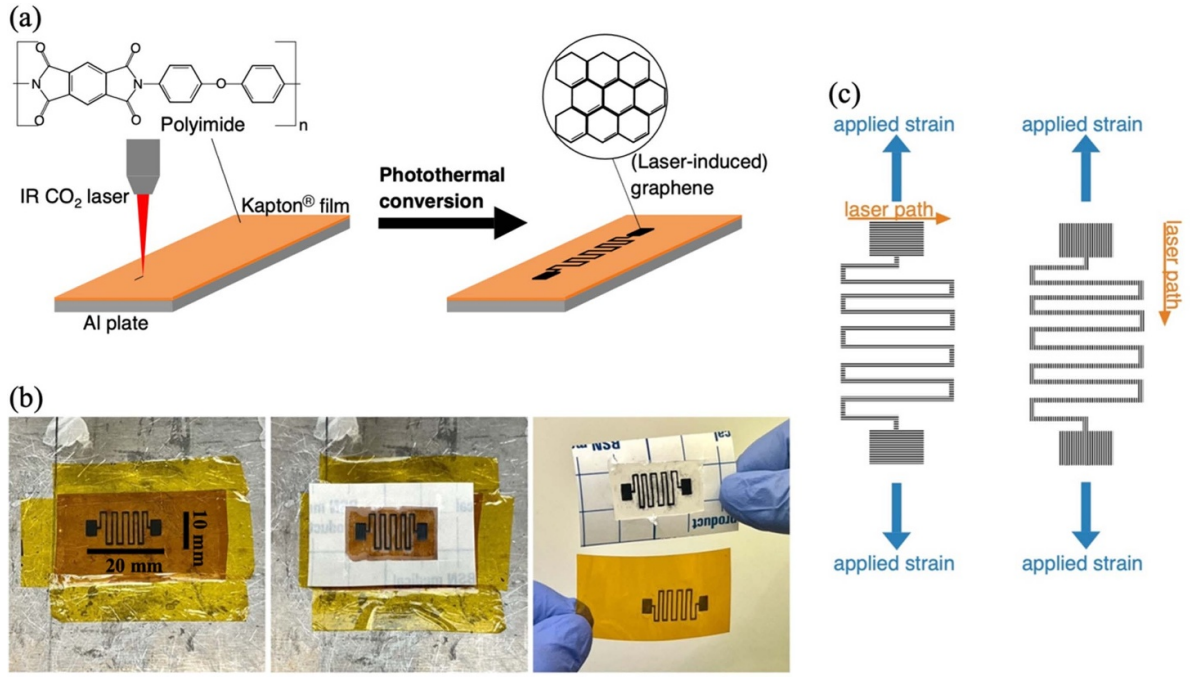

Figure 1. Fabrication process. (a) Scheme of LIG fabrication, illustrating the irradiation of a polyimide film (Kapton) that induces an *in-situ* conversion of disordered carbon into crystalline graphene. (b) Transfer process of LIG onto Fixomull, showing LIG on Kapton (left), Fixomull attached to Kapton (middle), LIG on Fixomull (upper right) and residual LIG on Kapton (lower right). Length scales are included for specification of the pattern dimensions in the left picture. (c) Scheme of the perpendicular (left) and parallel (right) configuration of lasing direction relative to application of strain.

LIG structures. This, in turn, induces a major relative resistance change and ultimately a large gauge factor.

2.2. Characterization tools and protocols

SEM has been applied to study the change of LIG morphology as a function of the applied strain. Images of the LIG/Fixomull stretch-release series (figures 2 and 3) were taken with an Inspect F50 (FEI company, United States) at an acceleration voltage of 5 kV. Imaging of the LIG/Fixomull samples under strain (figure 4) was performed with a FEI Verios 460 (FEI company, United States) at an acceleration voltage of 2 kV. All images were obtained through detection of secondary electrons.

For investigation of how the chemical structure of LIG changes with increasing applied strain, Raman spectroscopy was carried out at an LabRAM Odyssey tool (HORIBA, Japan). Spectra were taken with a laser wavelength of $\lambda = 532$ nm, a magnification lens of 10x, an 1800 lines/mm grating, a ND filter of 50%, an acquisition time of 20 s and 3 accumulations.

Van der Pauw measurements were performed to determine the sheet resistance of the stretched and released LIG/Fixomull samples. For this purpose, LIG samples with the shape of Greek crosses, composed of two perpendicularly criss-crossed 3×1 mm^2 beams with 1.4×1.4 mm^2 large squares at each end, were fabricated. The used instruments were a Karl Suss PSM 6 probe station (SUSS MicroTec SE, Germany) connected to an Agilent semiconductor parameter analyzer unit (Agilent Technologies, United States), controlled via the EasyEXPERT software. The current range was swept from 0 to 1 mA with a step size of 10 μA.

The sheet resistance $R_{CD,AB}$ was calculated by inserting the voltage drop measured across two adjacent contacts A and B ΔV_{AB} into the following equation [32]:

$$R_S = \frac{\pi}{\ln(2)} \frac{\Delta V_{AB}}{I_{CD}} \quad (1)$$

where I_{CD} is the current applied between the two opposing contacts C and D. For each parameter set, the average of the two theoretically equal values $R_{CD,AB}$ and $R_{AB,CD}$ was plotted. For each strain level, three samples were measured, and the average of the values was provided in the graphs, including their corresponding calculated standard deviation.

Lastly, the LIG/Fixomull sensor was characterized electromechanically using the custom setup depicted in figure 7(a). Uniaxial tensile stress was applied by the manual push pull force gauge equipped with a digital display to control the displacement. Simultaneous electrical measurements were conducted with an Autolab PGSTAT204 potentiostat/galvanostat instrument (Metrohm, Switzerland) in a two-electrode configuration (with reference and working electrodes being identical), which was controlled by the corresponding NOVA 2.1.3 software (Metrohm Autolab B.V., Netherlands). Both measurements, LSV and chronoamperometry were conducted in potentiostatic mode. For LSV, the potential was swept from -1 V to 5 V at a scan rate of 0.1 V s^{-1} and a step size of 0.01 V.

A total of six measurements, i.e. three strain-release cycles were performed for each strain level. For chronoamperometry, a constant potential of 1 V was applied while the sample was subjected to three consecutive strain-release cycles with a dwell time of 200 s in each state to enable signal stabilization. An additional measurement over 20 strain-release cycles was performed for the 30% strain level. Data evaluation comprised calculation of resistance values from the output *V*–*I*-data by applying Ohm's law. The resistance values with their corresponding strain information were used for determination of the strain-dependent gauge factor (GF) according to the following equation [16]:

$$\mathrm{GF} = \frac{\Delta R/R_0}{\Delta L/L_0} \tag{2}$$

with resistance in released state R_0, change in resistance due to stretching ΔR, original sensor length L_0 and elongation ΔL.

3. Results and discussion

3.1. Structural characterization of LIG transferred to polyurethane

SEM images in figure 2 illustrate the morphological evolution of LIG upon application and subsequent release of tensile stress.

Images in figure 2(a) (after laser writing, on Kapton) and 2(b) (after transfer to Fixomull) reveal the severe crack formation on the LIG pattern upon transfer from Kapton to Fixomull, creating a clearly visible island structure. The level of rupture is similar for strains between 5% and 30% (figure 2(c)–(h)): LIG islands are still in place, maintaining an ordered, even structure, which indicates restoration of the graphene pattern after application of strain. This situation changes with further increasing the strain to 40% and 60% (figures 2(i) and (j)): the cracks are deepening, and more and more individual LIG islands are displaced, arousing a cragged structure with LIG islands, detached from the Fixomull substrate, on top. For a strain level of 80% (figure 2(k)), the upper LIG layer is fully detached in some parts, causing an increased density of cracked LIG pieces and exposure of an underlying layer.

SEM images of higher magnification for LIG on Kapton and LIG/Fixomull for the strain levels of 5%, 30% and 80% are shown in figure 3. First of all, these images illustrate the loss of the fibrous morphology of LIG upon its transfer from Kapton to Fixomull. While figure 3(a) shows the fibers of LIG, produced upon the laser irradiation on Kapton, figures 3(b)–(d) show that the characteristic LIG landscape of graphene flakes, forming a porous network has been preserved after transfer. However, the fibers are not visible anymore since they were trapped on the Fixomull surface during the transfer process. Besides, it was observed that for imaging areas within the boundaries of the LIG islands observed in figure 2, defined by the cracks, the morphology of relaxed LIG pores does not change distinctly after application of strain. That is to say, the fundamental porous structure of the LIG is restored upon relaxation even after application of 80% strain (figure 3(d)).

Additionally, we performed a SEM characterization of LIG under strain (5%, 30%, 80%) to investigate the pore structure while tensile stress is applied. Low magnification SEM images (figures 4(a)–(c)) again clearly illustrate the transition from a LIG island structure at low-moderate strain (up to 30%) to a visibly disordered, cragged pattern at high strain (80%). Higher magnification images (figures 4(d)–(f)) give deeper insights into this evolution, depicting a porous, unperturbed, well-connected LIG network with only few small cracks at a strain of 5%. At 30% strain, certain elongation of the flakes is noticed in some parts, and cracks open up, yet, only to a degree at which a fundamental interconnection of the pattern is still maintained. At a strain level of 80%, LIG flakes are heavily elongated, making the conductive network prone to partial rupture.

Overall, the SEM images reveal a severe morphological change owing to the peel-off transfer of LIG. Yet, a functional degradation of the sensor pattern in the sense of heavily interrupted conductive pathways is only developed under application of high strain, as it will be observed in the electromechanical performance section. Similarly, Kammarchedu *et al* reported on reliable sensing performance despite the loss of primary morphological characteristics upon LIG transfer. To be more explicit, they observed fiber degradation upon transfer which however does not destroy the conductive network as the fibrous morphology in the first place ensures preservation of a well-connected (and thus conductive) structure. The reason is to be found in the fibers' high surface area that strengthens adhesion to the target substrate [16].

By means of Raman spectra (figure 5(a)), the evolution of chemical structure of LIG as a function of strain is depicted. The first difference is the increment of the D peak intensity for the LIG transferred to Fixomull compared to the LIG on PI due to the increase of disorder caused by the peel-off process. For strains between 5% and 30%, despite small fluctuations, the spectra are similarly displaying a 2D peak with reduced intensity and broadened D and G peaks with I_D/I_G ratios close to 1, indicating an akin level of disorder induced inside this range of strain values. A clear change in the spectra catches the eye for increasing the strain from 30% to 40%: The 2D peak intensity becomes vanishingly small, while the width of the D and G peaks increases significantly, almost causing the D and G peaks to merge. Band broadening and consequently the noticeable convolution of D and G peak are typical indications of an increasing defect density in the crystal lattice [33, 34], which, in the present case, is caused by application of a high level of strain. These phenomena intensify such that the spectra of the 60% and 80% stretched samples are more similar to the one of amorphous carbon [33] than to the one of multilayer graphene, which will doubtlessly affect the electrical properties of the material.

Besides, analysis of the peak positions is very insightful since the vibrational frequency is directly related to changes in atomic positions as predicted by the dispersion relation [35]. Application of tensile stress causes the interatomic distance of

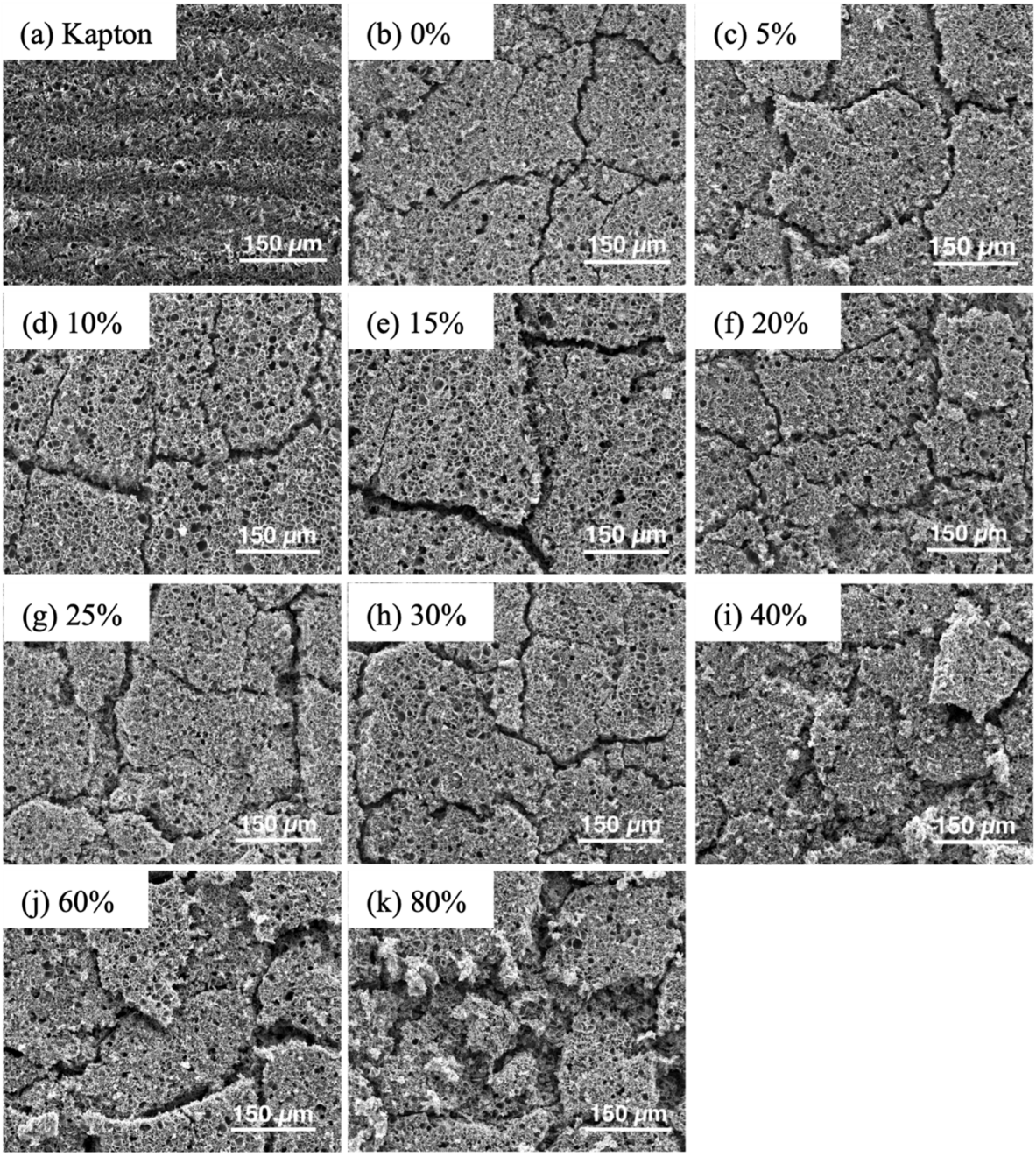

Figure 2. SEM images of the stretching series including LIG on Kapton (a), LIG transferred to Fixomull (b) and LIG/Fixomull after three consecutive stretch-release cycles to the specified strain level ((c)–(k)). All SEM images were taken with a magnification of x500.

the C-atoms to increase which in turn will result in a decrease of vibrational frequency-a red shift of Raman bands [36]. As can be seen in figure 5(b), the G mode of LIG is red shifted by $\sim$13 cm^{-1} for transferring LIG from Kapton to Fixomull (referred to as 0% in the graph), which can be explained by the tensile strain induced during peel-off. For transferred and 5%–30% strained+released LIG samples, peak positions remain similar, which indicates restoration of the initial, functional structure after relaxation from moderate strains up to 30%. After application of larger strains, i.e. 40%, 60% and 80% strained+released LIG samples, the G mode is blue shifted which seems contradictory at first as a larger red shift would be expected for larger tensile strain. However, as it has been proven by Wu *et al*, the G band position is sensitive to several external factors, such as doping, an altered interface coupling and any type of lattice distortion [33]. For graphene specifically, a high amount of sp^3-like defects in the lattice causes the G peak to blue shift [33]. In line with the overall picture of the 40%, 60% and 80% strains Raman spectra (figure 5(a)), the observed blue shift (figure 5(b)) confirms the assumption of a strain-induced amorphization of graphene.

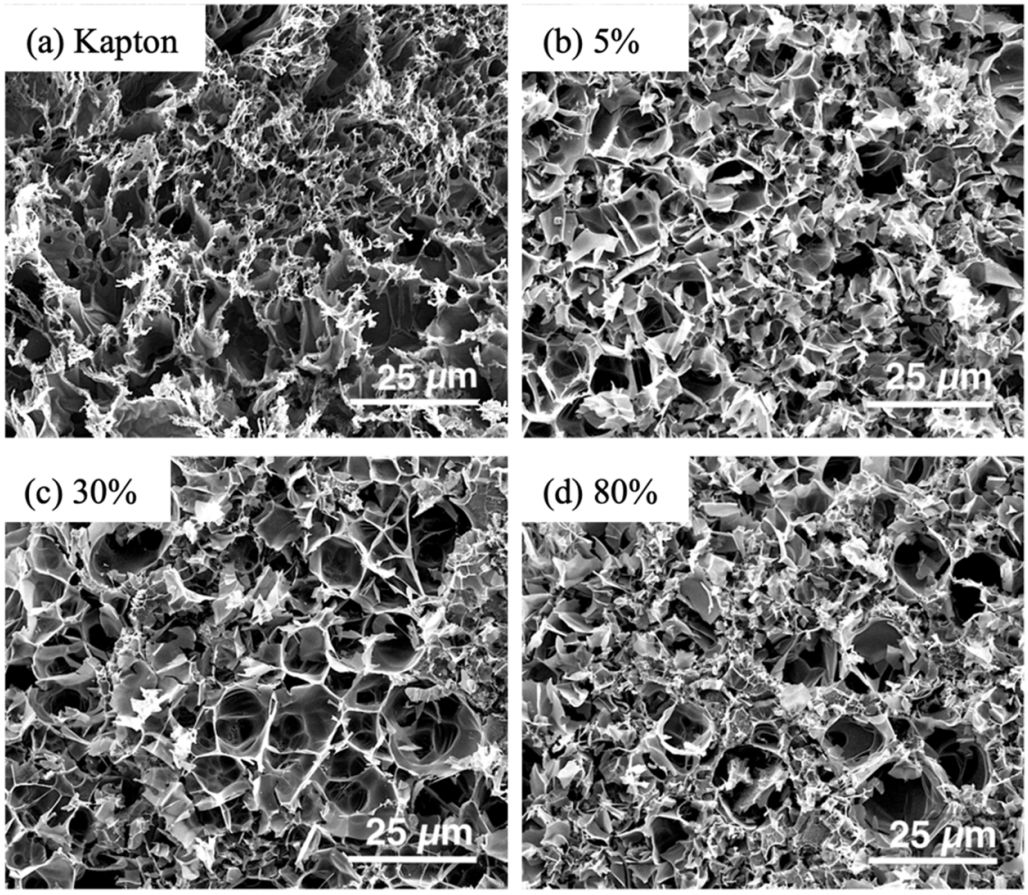

Figure 3. SEM images of the stretching series including LIG on Kapton (a) and LIG/Fixomull after three consecutive stretch-release cycles to the specified strain level (b)–(d). All SEM images were taken with magnification of x3000.

3.2. Electrical characterization of LIG transferred to polyurethane

Fixomull alone, whose main component is polyurethane, is an electrical insulator. In contrast, LIG is, thanks to its conjugated π-system, electrically conductive with a conductivity of $\sim$2500–3000 S m^{-1} as reported by Pinheiro *et al* [37]. The mechanism of charge carrier mobility in polyurethane is not changed upon transfer of the LIG as the insulator does not affect the conduction process in a direct manner. However, as the substrate on which LIG lies, it indirectly reduces the overall charge carrier mobility of the LIG/polyurethane system when the conductive pathways of LIG are for the first time partially interrupted upon transfer to polyurethane. Later, with increasing strain, more conductive pathways will be interrupted, exposing insulating polyurethane, and thereby further reducing overall charge carrier mobility. Altogether, the reduction of charge carrier mobility in LIG is the crucial process. The correlation between the changes in the charge carrier mobility in LIG, first after transfer from polyimide to polyurethane and second, as a function of the strain level, was characterized in this work by the changes in the electrical properties through sheet resistance measurements.

Electrical characterization by van der Pauw technique yielded the strain-dependent sheet resistance as given in figure 6, with the points indicating the average value of measurements performed on three different LIG samples for each strain and the vertical dashed lines, the corresponding standard deviation.

The low sheet resistance of 11.35 ($\pm$0.44) Ω/sq for LIG on Kapton indicates formation of highly conductive graphene. In line with the findings from Raman G band position analysis (figure 5(b)) and investigations by Dallinger *et al* [10], a distinct increase of sheet resistance by factor 10 was registered for the transition of LIG from Kapton to Fixomull, due to the structural change brought about by peel-off transfer. The increasing sheet resistance upon increasing strain is related to an increasing number of defects that interrupt the effective conductive network. A maximum value of 244.90 ($\pm$106.35) Ω/sq was measured for 80% strained LIG on Fixomull. The increase of the sheet resistance by factor 10 caused after peeling-off the LIG from the original Kapton substrate is drastic in comparison to the similar sheet resistance values after transfer for up to 15% of strain and the moderate rise by factor 2 for 20%–80% of strain. This result is in accordance with the observations from SEM characterization (section 3.1): for strained and relaxed LIG, changes in morphology and electrical performance are most pronounced for the switch from LIG on Kapton to LIG on Fixomull. Although degradation is advancing with increasing the applied tensile

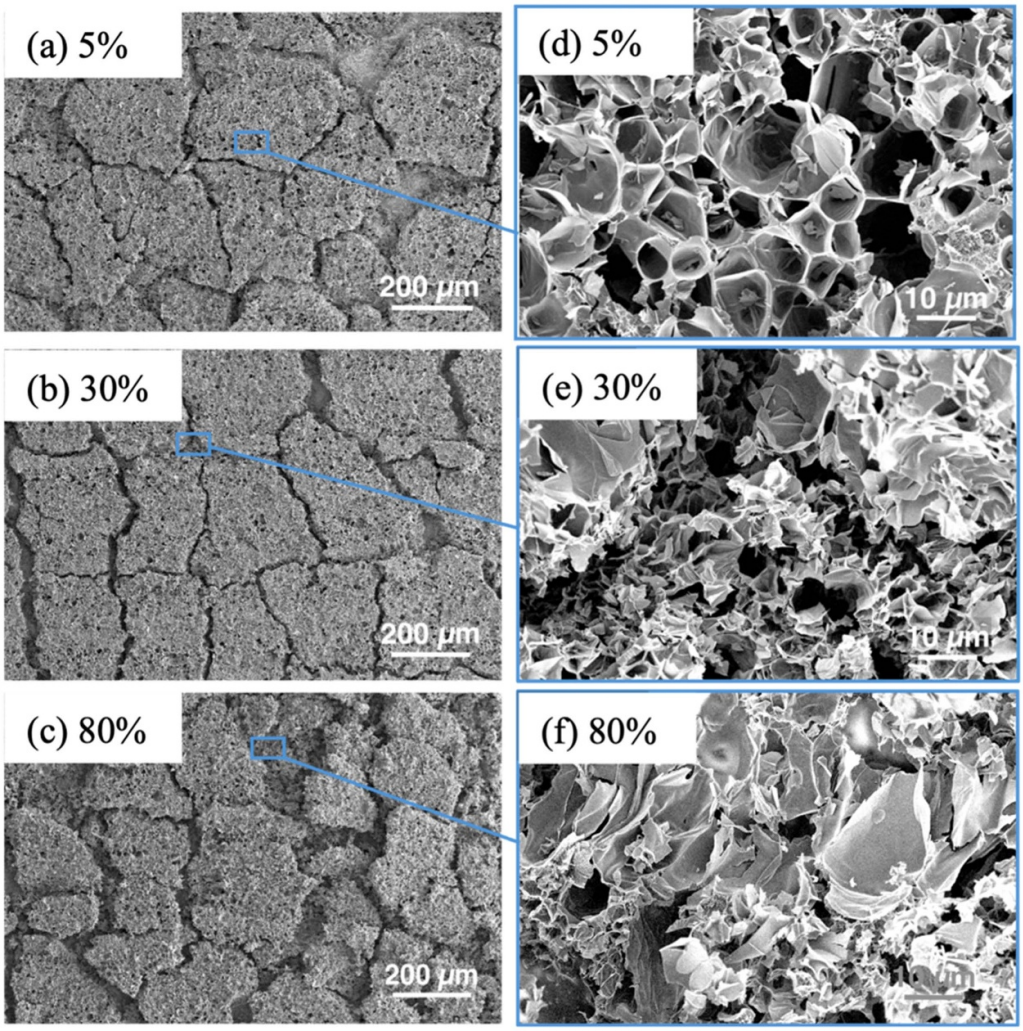

Figure 4. SEM images of transferred LIG onto Fixomull while being strained by 5% (top row), 30% (middle row) and 80% (bottom row). Images (a)–(c) were taken with magnification of x100, with blue boxes inserted to indicate the sections that are displayed with a magnification of x1500 in images (d)–(f).

stress, the relaxed LIG remains (partly) functional and structurally intact even after being strained by 80%.

Standard deviations of the measured sheet resistances were observed to be growing with strain. This can be considered as a sign of an intensification of the inherently inhomogeneous nature of LIG [26] under high strain.

3.3. Electromechanical performance of LIG/Fixomull sensor devices

The following section outlines important performance parameters of strain sensors, including gauge factor, linearity, response and recovery time and stability/reproducibility, to allow a general placement of our strain sensors.

Figure 7(a) shows an image of the experimental setup used for the electromechanical characterization of the devices, outlined in section 2.2 *Characterization devices and protocols*, with close up images of one of the sensors in the initial state (figure 7(b)) and under strain (figure 7(c)).

The key measure to evaluate a strain sensor's sensitivity, the gauge factor, was investigated as a function of strain (figure 8(a)). A gauge factor of 7.48 is obtained for a strain of 5%. A slight decrease of the gauge factor is noticed for an increase of the strain to 15%, followed by fairly constant values up to 30% strain and another rise for straining up to 60%. A remarkably higher gauge factor with extraordinarily high standard deviation was yielded for a strain of 80%, embodying the severe and partly irreversible damage of the LIG pattern at that strain level. The comparably low gauge factor at low-medium strain is a sign of preferential formation of microcracks that will reconnect upon relaxation. Consequently, this strain sensor will be able to resist high strains as opposed to strain sensors with very high gauge factors at low strain already indicating increased formation of larger, irreversible cracks that interrupt the current flow along the conductive LIG pathway.

Figure 8(b) shows the relative resistance change as a function of strain with a linear regression line inserted under consideration of strains up to 30% to determine the linear

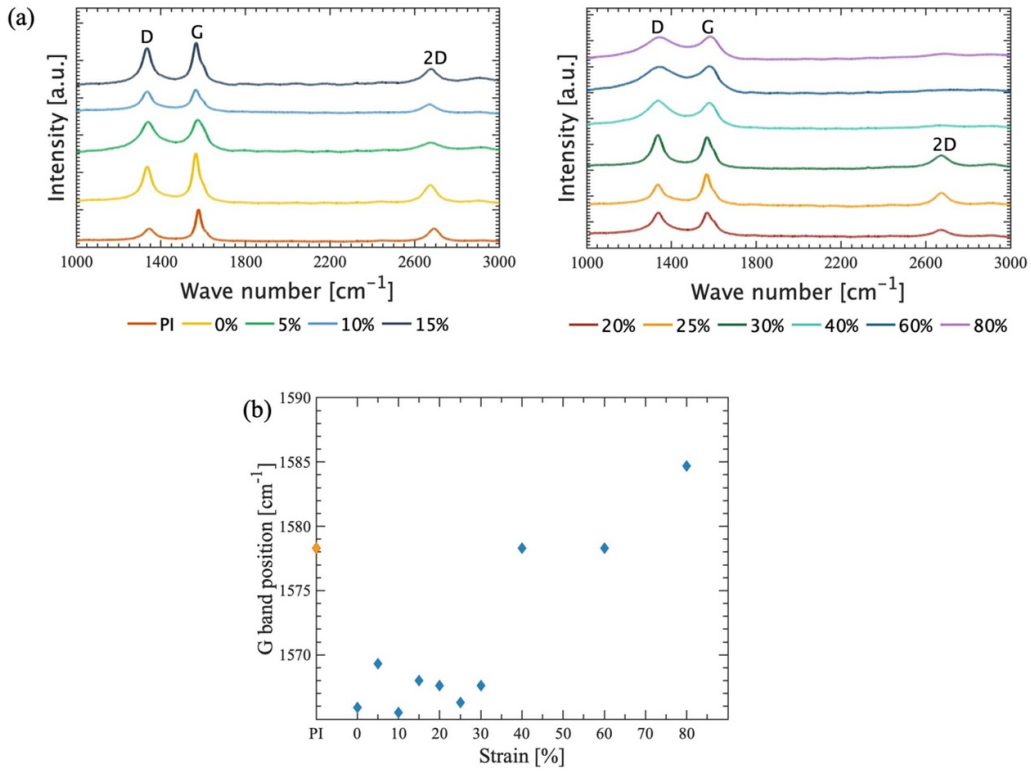

Figure 5. (a) Raman spectra of the samples including LIG on Kapton (corresponding to the spectrum denominated PI), LIG transferred to Fixomull (corresponding to the 0% spectrum) and LIG/Fixomull at different strain levels (from 5% to 80%). The spectra of the 5%–80% strain values were taken from the relaxed sample after it was exposed to three consecutive stretch-release cycles to the specified strain level, all indicated in the legends below the graphs. The spectra were divided into 2 graphs, left and right, in order to facilitate the correct visualization of all of them within a sensible size. In addition, all the spectra are represented at the same scale, but they are just displaced along the vertical direction to facilitate again their visualization and comparison. (b) Position of the G band as a function of the strain applied to the LIG samples. The G band position of LIG on Kapton is inserted in orange at the left, on the *y*-axis.

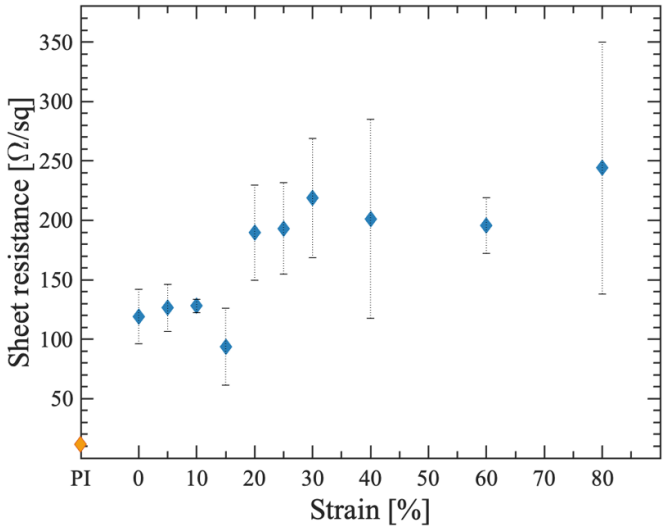

Figure 6. Van der Pauw sheet resistance as a function of the strain applied to the LIG sample. Each point represents the average value of measurements performed on three different LIG samples. Vertical dashed lines represent the standard deviation of each sample set. The sheet resistance of LIG on Kapton is inserted in orange at the left, on the *y*-axis.

measurement range of the developed sensor. Our sensor shows linear behavior reliably up to a strain of 30% and a close-to-linear relationship between sensor output signals and applied strain up to a strain of 60%.

To further investigate the temporal connection between application of tensile stress and sensor response, figure 8(c) provides an extract from the threefold strain-release cycle to 30% strain (figure 9(f)), revealing an exponential relaxation

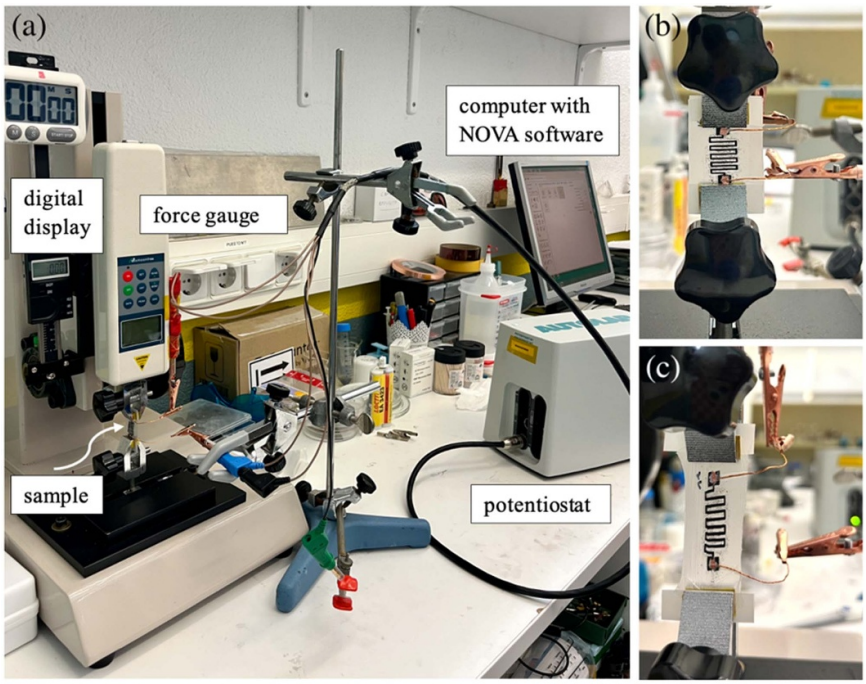

Figure 7. (a) Custom setup used to perform simultaneously strain with the force gauge and linear sweep voltammetry and chronoamperometry experiments with the potentiostat/galvanostat. Close-ups of the sensor sample, mounted in the force gauge and connected to the potentiostat/galvanostat in initial (b) and strained (c) states.

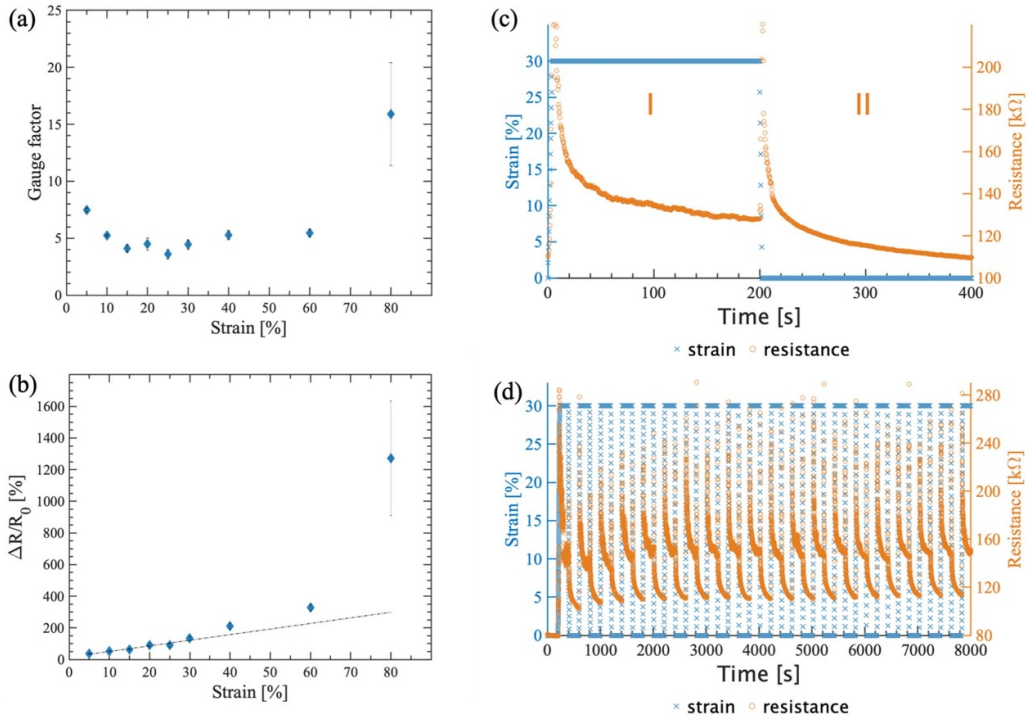

Figure 8. Electromechanical performance of the sensors encapsulated in Fixomull. (a) Gauge factor as a function of strain. The data points represent the average of three consecutive linear sweep voltammetry measurements with the standard deviation marked as vertical dotted line. (b) Relative resistance change $\Delta R/R_0$ as a function of strain depicting the linear regime with the linear regression line including strains up to 30%. (c) One stretch-release cycle from the 30% cycling (figure 9(f)) used for determination of τ time constants. The left section (I) and the right section (II) were fit exponentially to determine τ_{response} and τ_{recovery}, respectively. (d) Cyclic behavior during 20 subsequent stretch-release cycles to 30% strain.

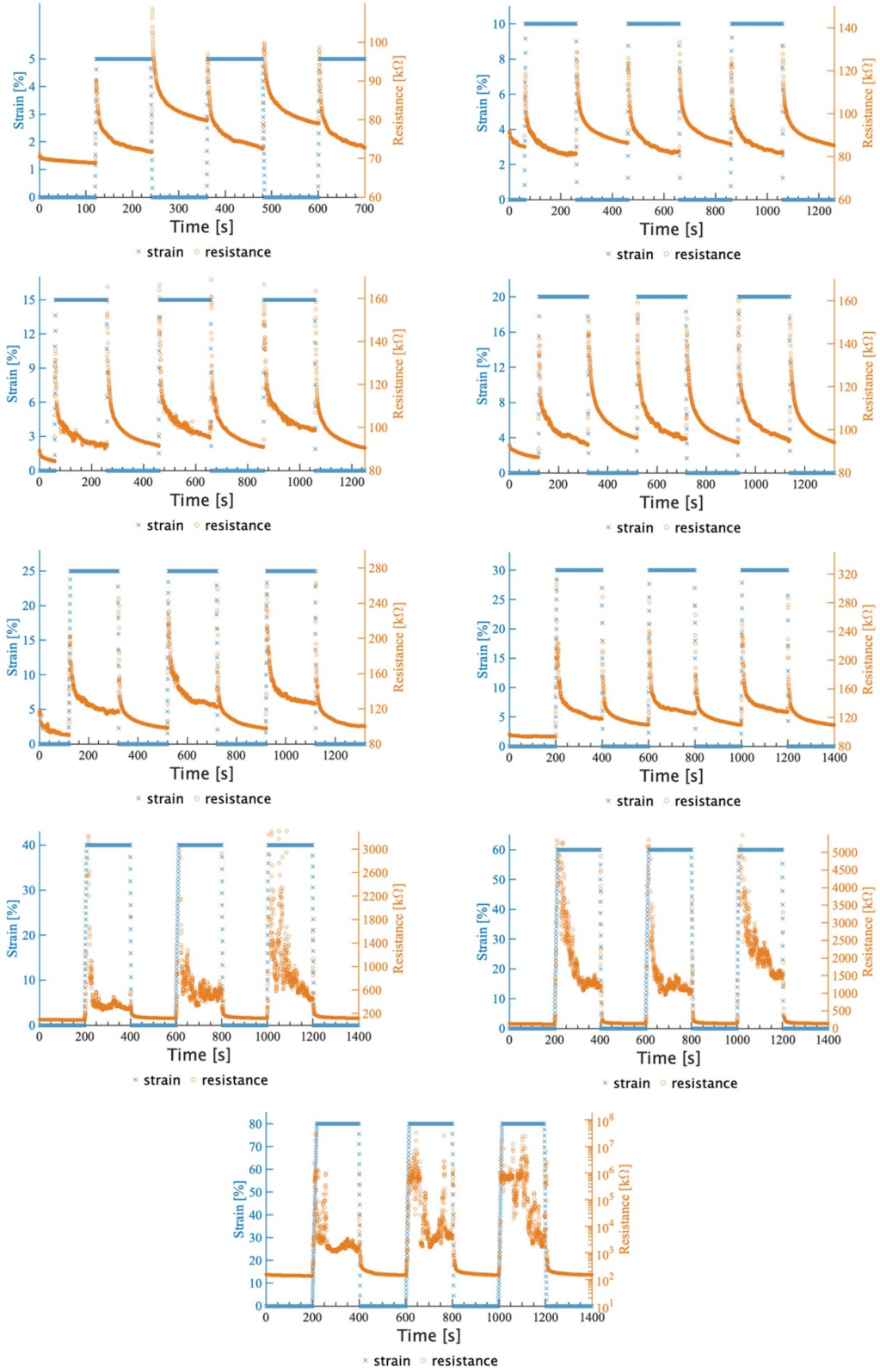

Figure 9. Cyclic tests for the whole stretching series depicting the change in electrical resistance (orange line) as a function of time upon threefold stretch–release to the strain level (blue line) specified in each plot.

behavior of the form $A^{*}\exp(-t/\tau)$ for both the stretched (curve I in figure 8(c)) and released state (labeled as II in figure 8(c)). Correspondingly, 2 different time constants to describe the relaxation behavior in both states were determined and given for each strain level in table S1 (supplementary data file). As the resistance did not clearly stabilize in strained state for

Table 1. Comparison of the performance characteristics of the LIG/Fixomull strain sensor studied in this work with similar LIG/MPU and LIG/PDMS devices obtained from other works in the literature.

Material system	Linear regime	Gauge factor	Response time	Stretch-ability	Cyclability	References
LIG/MPU	min. 0%–30%	3.5–7.5	∼16 s	min. 80%	20 cycles to $\varepsilon = 30\%$	This study
	0%–50%	5–7	>18 s	min. 100%	10 000 cycles to $\varepsilon = 5\%$	[16]
	0%–40%	/	21 s	min. 100%	200 cycles to $\varepsilon = 30\%$	[17]
	0%–30%	Up to 25 for fibrous LIG, up to 70 for porous LIG	18.5 s	min. 100%	200 cycles to $\varepsilon = 30\%$	[10]
LIG/PDMS	0%–1.6%	111	1040 ms	/	1500 cycles to $\varepsilon = 8\%$	[20]
	/	160	70 ms	30%	/	[8]
	/	15.8 (for $\varepsilon = 10\%$–20%)	1160 ms	/	2000 cycles to $\varepsilon = 5\%$	[21]

strains $\geqslant$40%, no time constants $\tau_{response}$ could be specified for these strain levels. For strains $\leqslant$30%, the time constants for substrate recovery in stretched and relaxed state do not differ greatly from one another, which is founded in the viscoelastic character of MPU: an exponential stress relaxation at constant elongation after a sudden change of the strain state is characteristic of viscoelastic materials [38] and mirrored in the time response of the resistance as proven by Dallinger *et al* [10]. Second, this result reinforces the obtained ones from SEM and Raman characterization: similar level of degradation in the properties and strong endurance of the LIG structure integrity for that range of strains.

The twenty-fold repetitive stretch-and-release to 30% strain cycling (figure 8(d)) suggests stable continuous monitoring capabilities of the developed sensor up to this strain level. As can be seen in figure 8(d), the resistance in strained state levels off at ∼145 (±3) kΩ and in released state, at ∼111 kΩ (±2) after a short, initial stabilization. Compared to cyclability tests of different LIG-based strain sensors, this result stands out as most studies limit the maximum strain application in such tests to 10% [16, 20, 21]. The limiting number of cycles equal to 20 is due to the manual nature of the force gauge setup, which would have meant a considerable amount of time consumption for very long cycling. In this case, our main purpose was to show, rather than the endurability or the lifetime of the device, its reproducible performance under a significant strain level, inside the linear regime.

Cyclic tests give information about signal stability and the time component of the sensor response. Figure 9 shows a series of plots depicting the change in electrical resistance (orange line) as a function of time upon repeated stretching to the strain level (blue line) specified in each plot. The signal stability of the sensor is visibly reduced when applying strains $\geqslant$40%. Up to a strain of 30% (figures 9(a)–(f)), a stable resistance is recovered within the time span of 200 s for both the strained and released state of the sensor, while the resistance in strained state does not stabilize anymore for repeated straining to 40%, 60% and 80% (figures 9(g)–(i)) within 200 s. However, the excellent ability of the sensor to recover even from high strain is embodied in the restoration of a stable resistance value in the relaxed state (figures 9(g)–(i)). These observations coincide with the identified up to 30% linear regime of the sensor.

The performance evaluation depicts the expectable trade-off between key parameters sensitivity and stretchability. The parameter to be optimized depends on the desired sensor application; primarily on whether it is intended to monitor small strain (e.g. physiological signals), which would require high sensitivity, or to monitor large strain (e.g. joint movement), which would require high stretchability. In order to record certain body movements, tolerance of high strain up to 100% may be required [1, 16]. The sensor produced in this work shows ohmic behavior, i.e. the required electrical characteristic up to high strain of 80% for the first strain cycles for which the LIG pattern is largely restored, hence functionality recovered to a considerable extent. Yet, perfect linear *V*–*I*-behavior is slowly being lost upon repeated stretching to strains $\geqslant$60% (figure S2, supplementary data file), when LIG flakes do not withstand the heavy tensile strain anymore, causing irreversible structural damage to the conductive LIG pattern.

Summing up the findings of the electromechanical measurements, the linear regime was found to comprise strains up to 30%. In this region, the sensor's output signals are linearly related to the applied strain and both the resistance in strained and in relaxed states are restored for twenty-fold repetition of strain-release cycles. For strains between 30% and 60%, the response of the sensor cannot be considered clearly linear anymore. Nonetheless, the *V*–*I*-behavior is still perfectly linear (figure S2, supplementary data file), the resistance in relaxed state fully stabilizes and in strained state, roughly. For even larger strains, the sensor response is becoming clearly non-linear and the resistance in strained state fluctuates heavily. The results are in line with the ones of Keller *et al* who identified full recovery of LIG/Fixomull sensors for cyclic stretching to 30% and restoring of functionality for relaxation after straining up to 100% [17].

Table 1 presents a comparison of the performance parameters determined for the sensor developed in this study with LIG/MPU and LIG/PDMS sensors found in the literature. These findings clearly point out the major differences

between LIG/MPU and the way more researched LIG/PDMS skin sensors with respect to electromechanical behavior. LIG/PDMS strain sensors usually stand out due to their high gauge factor (well above 100), which allows to register smaller strain changes precisely within milliseconds (low response and recovery time) [20] for a high number of repetition cycles. In contrast, LIG/MPU strain sensors possess significantly larger linear regimes and high stretchabilities, predestining them for high strain applications. To be more explicit, the LIG/Fixomull sensor developed in this work shows linearity to at least 30% strain and stretchability to 80%. These values give an idea of the versatile application possibilities of our proposed sensor, since a large number of movements from different parts of the human body that are interesting to be monitored fall within the sensor's working range. On the bottom line, LIG/MPU and LIG/PDMS sensors complement one another such that both sensors cover the monitoring of the desired motion: from subtle physiological signals to large-scale limb movements.

4. Conclusion

This study investigates the morphological and electromechanical changes underwent by LIG upon transferring it to Fixomull (MPU) and subsequently applying different levels of strain. Owing to the structure-property correlation, this work provides a better understanding of the functionality of LIG-based strain sensors, which are recently attracting a lot of attention due to their huge potential for IoT-related applications.

SEM images revealed that the most damaging step was the transfer of the LIG from Kapton to Fixomull by peel-off method, which exerts a high tensile stress on the porous LIG, thereby generating a pattern of LIG islands surrounded by cracks. An intensified interruption of the conductive LIG pathways upon application of increasing strain, but with a great capacity of structural integrity maintenance inside the islands, was observed for strains in the range of 5% to 60%. At a strain level of 80%, the LIG pores could not withstand the tensile strain for a prolonged time and as result, the structure ended clearly destroyed. Corresponding Raman spectra exhibit a vanishing 2D peak intensity and significant convolution of D and G peaks for straining the LIG to $\geqslant$40%, suggesting the amorphization of highly strained LIG. Besides, van der Pauw sheet resistance measurements showed an increasing value with increasing strain to the following extent: One order of magnitude from 11.35 ($\pm$0.44) Ω/sq to 119.11 ($\pm$22.87) Ω/sq upon transfer to Fixomull, similar values after transfer for up to 15% strain and a moderate rise by factor 2–244.00 ($\pm$106.00) Ω/sq for the strain range from 20% to 80%.

Eventually, our low-cost and straightforwardly produced LIG/Fixomull strain sensor was investigated electromechanically, resulting in a high linearity up to 30% and reliable data acquisition up to 60% strain. A gauge factor of 7.48 was determined for a strain of 5%. For the 10%–60% strain range, the gauge factor was found to remain at a constant level of $\sim$4.5 before a significant rise to 15.90 was identified for a strain of 80%, with a remarkably high standard deviation. These results are in good accordance with the preceding material characterization which revealed functional degradation of the sensor at 80% strain due to the collapse of the conductive three-dimensional LIG network under sustained tensile load. At last, a cyclic test demonstrated stable signal output for 20 subsequent stretch-release cycles to 30% strain.

Overall, Fixomull proved to be an attractive substrate material for LIG-based sensing devices, especially considered as complement to LIG/PDMS sensors. Addressing the remaining issue of significant crack formation upon LIG transfer from Kapton to Fixomull will improve the sensor's performance with regard to sensitivity and stretchability even further.

Data availability statement

The data that support the findings of this study are available upon reasonable request from the authors.

Acknowledgment

This study was funded by project PID2023-146988OB-C22 by MCIU/AEI /10.13039/501100011033/FEDER, UE. We acknowledge the service from the MiNa Laboratory at IMN, and funding from CM (project S2018/NMT-4291 TEC2SPACE), MINECO (project CSIC13-4E-1794) and EU (FEDER, FSE). The authors also would like to acknowledge ICTS Micronanofabs.

Conflict of interest

The authors declare no conflicts of interest.

Author contributions

Cornelia Hoppe 0009-0003-2557-7885
Conceptualization (lead), Data curation (lead), Formal analysis (lead), Investigation (lead), Methodology (lead), Writing – original draft (lead)

Yu Kyoung Ryu 0000-0002-5000-2974
Conceptualization (lead), Formal analysis (lead), Methodology (lead), Supervision (lead), Writing – review & editing (lead)

Javier Martinez 0000-0002-5912-1128
Funding acquisition (lead), Supervision (lead), Validation (lead), Writing – review & editing (lead)

References

[1] Yoon H, Lee K, Shin H, Jeong S, Lee Y J, Yang S and Lee S H 2023 *In situ* co-transformation of reduced graphene oxide embedded in laser-induced graphene and full-range on-body strain sensor *Adv. Funct. Mater.* **33** 2300322

[2] Tang L, Wu S, Qu J, Gong L and Tang J 2020 A review of conductive hydrogel used in flexible strain sensor *Materials* **13** 3947

[3] Huang C, Wang J, Wang S and Zhang Y 2023 Internet of medical things: a systematic review *Neurocomputing* **557** 126719

[4] Malhotra P, Singh Y, Anand P, Bangotra D K, Singh P K and Hong W-C 2021 Internet of things: evolution, concerns and security challenges *Sensors* **21** 1809

[5] Khalid M A U and Chang S H 2022 Flexible strain sensors for wearable applications fabricated using novel functional nanocomposites: a review *Compos. Struct.* **284** 115214

[6] Liu X, Miao J, Fan Q, Zhang W, Zuo X, Tian M, Zhu S, Zhang X and Qu L 2022 Recent progress on smart fiber and textile based wearable strain sensors: materials, fabrications and applications *Adv. Fiber Mater.* **4** 361–89

[7] Kaidarova A and Kosel J 2021 Physical sensors based on laser-induced graphene: a review *IEEE Sens. J.* **21** 12426–43

[8] Jeong S-Y, Ma Y-W, Lee J-U, Je G-J and Shin B-S 2019 Flexible and highly sensitive strain sensor based on laser-induced graphene pattern fabricated by 355 nm pulsed laser *Sensors* **19** 4867

[9] Luo Y, Zhu B, Zhang S, Zhang P, Li X, Wang L, Lu B and Travas-Sejdic J 2022 Stretchable and flexible non-enzymatic glucose sensor based on poly(ether sulfone)-derived laser-induced graphene for wearable skin diagnostics *Adv. Mater. Technol.* **7** 2101571

[10] Dallinger A, Keller K, Fitzek H and Greco F 2020 Stretchable and skin-conformable conductors based on polyurethane/laser-induced graphene *ACS Appl. Mater. Interfaces* **12** 19855–65

[11] Lin J, Peng Z, Liu Y, Ruiz-Zepeda F, Ye R, Samuel E L G, Yacaman M J, Yakobson B I and Tour J M 2014 Laser-induced porous graphene films from commercial polymers *Nat. Commun.* **5** 5714

[12] Allen M J, Tung V C and Kaner R B 2010 Honeycomb carbon: a review of graphene *Chem. Rev.* **110** 132–45

[13] Bonaccorso F, Colombo L, Yu G, Stoller M, Tozzini V, Ferrari A C, Ruoff R S and Pellegrini V 2015 Graphene, related two-dimensional crystals, and hybrid systems for energy conversion and storage *Science* **347** 6217

[14] Swatantra P S, Li Y, Be'er A, Oren Y, Tour J M and Arnusch C J 2017 Laser-induced graphene layers and electrodes prevents microbial fouling and exerts antimicrobial action *ACS Appl. Mater. Interfaces* **9** 18238–47

[15] Velasco A, Ryu Y K, Boscá A, Ladrón-de-guevara A, Hunt E, Zuo J, Pedrós J, Calle F and Martinez J 2021 Recent trends in graphene supercapacitors: from large area to microsupercapacitors *Sustain. Energy Fuels* **5** 1235–54

[16] Kammarchedu V, AlSiyabi M and Ebrahimi A 2025 Skin-conformal myography for real-time hand tracking using a laser-induced graphene strain sensor array *Adv. Intell. Syst.* **7** 2400812

[17] Keller K, Grafinger D and Greco F 2021 Printed and laser-scribed stretchable conductors on thin elastomers for soft and wearable electronics *Front. Mater.* **8** 688133

[18] Bolotin K I, Sikes K J, Jiang Z, Klima M, Fudenberg G, Hone J, Kim P and Stormer H L 2008 Ultrahigh electron mobility in suspended graphene *Solid State Commun.* **146** 351–5

[19] Ferrari L M, Taccola S, Barsotti J, Mattoli V and Greco F 2020 *Ultraconformable Organic Devices. Organic Flexible Electronics* (Woodhead Publishing) pp 48–478

[20] Barja A M, Ryu Y K, Tarancón S, Tejado E, Hamada A, Velasco A and Martinez J 2024 Laser-induced graphene strain sensors for body movement monitoring *ACS Omega* **9** 38359–70

[21] Yen Y-H, Hsu C-S, Lei Z-Y, Wang H-J, SU C-Y, Dai C-L and Tsai Y-C 2022 Laser-induced graphene stretchable strain sensor with vertical and parallel patterns *Micromachines* **13** 1220

[22] Ma Z and Khoo B L 2024 Recent advances in laser-induced-graphene-based soft skin electronics for intelligent healthcare *Soft Sci.* **4** 26

[23] BSN medical GmbH *Leukoplast product: fixomull transparent* (available at: www.leukoplast.de/professionelles-produktsortiment/schuetzend-und-fixierend/fixierung/vollflaechige-fixierung/fixomull-transparent)

[24] D'Amora M, Lamberti A, Fontana M and Giordani S 2020 Toxicity assessment of laser-induced graphene by zebrafish during development *J. Phys. Mater.* **3** 034008

[25] Huang X *et al* 2022 Transient, implantable, ultrathin biofuel cells enabled by laser-induced graphene and gold nanoparticles composites *Nano Lett.* **22** 3447–56

[26] Velasco A, Ryu Y K, Hamada A, Andrés A, Calle F and Martinez J 2023 Laser-induced graphene microsupercapacitors: structure, quality, and performance *Nanomaterials* **13** 788

[27] Hamada A, Ryu Y K, Velasco A, Gómez-Mancebo M B, Carretero S F, Calle F and Martinez J 2025 Boosting flexible laser-induced graphene supercapacitors performance through double pass laser processing *iScience* **28** 111696

[28] Biswas R K, Farid N, O'Connor G and Scully P 2020 Improved conductivity of carbonized polyimide by CO_2 laser graphitization *J. Mater. Chem. C* **8** 4493–501

[29] Abdulhafez M, Tomaraei G N and Bedewy M 2021 Fluence-dependent morphological transitions in laser-induced graphene electrodes on polyimide substrates for flexible devices *ACS Appl. Nano Mater.* **4** 2973–86

[30] Zou Y *et al* 2023 Flexible wearable strain sensors based on laser-induced graphene for monitoring human physiological signals *Polymers* **15** 17

[31] Bisceglie A 2024 Cellulose acetate as novel precursor to synthesize laser induced graphene *MSc Thesis* Politecnico di Torino

[32] Cummins G and Desmulliez M P Y 2012 Inkjet printing of conductive materials: a review *Circuit World* **38** 193–213

[33] Wu J-B, Lin M-L, Cong X, Liu H-N and Tan P-H 2018 Raman spectroscopy of graphene-based materials and its applications in related devices *Chem. Soc. Rev.* **47** 1822–73

[34] Childres I, Jauregui L, Park W, Caoa H and Chena Y P 2013 Raman spectroscopy of graphene and related materials *New Developments in Photon and Materials Research* (Nova Science Publishers) pp 403–18

[35] Miller G J 5.5: Vibrational States and Phonon Dispersion Curves (available at: https://chem.libretexts.org/Bookshelves/Inorganic_Chemistry/Chemical_Group_Theory_(Miller)/05%3A_Blochs_Theorem/5.05%3A_Vibrational_States_and_Phonon_Dispersion_Curves)

[36] Tuschel D 2019 Stress, strain, and Raman spectroscopy *Spectrosc. Online* **34** 9 (available at: https://www.spectroscopyonline.com/view/stress-strain-and-raman-spectroscopy)

[37] Pinheiro T, Vazão de Almeida H, Nunes D, Martins R and Fortunato E 2025 Integrated iontophoresis and sweat sensing via paper-derived laser-induced graphene soft conductors *Mater. Horiz.* **12** 8194–204

[38] Kanyanta V and Ivankovic A 2010 Mechanical characterisation of polyurethane elastomer for biomedical applications *J. Mech. Behav. Biomed. Mater.* **3** 51–62